Supplementary Information

Litchi-Like FeS_2@$FeSe_2$ Core-Shell Microspheres Anode in Sodium Ion Batteries for Large Capacity and Ultralong Cycle Life

Wenxi Zhao [a, b, c], Chunxian Guo[d], Chang Ming Li [a, c, d]*

[a]Institute for Clean Energy & Advanced Materials, Faculty of Materials and Energy, Southwest University, Chongqing 400715, P.R. China

[b]School of Electronic Information Engineering, Yangtze Normal University, Fuling, Chongqing 408100, P.R.China

[c]Chongqing Key Laboratory for Advanced Materials and Technologies of Clean Energies, Chongqing 400715, P.R. China

[d]Institute of Materials Science and Devices, Suzhou University of Science and technology, Suzhou, 215009, China

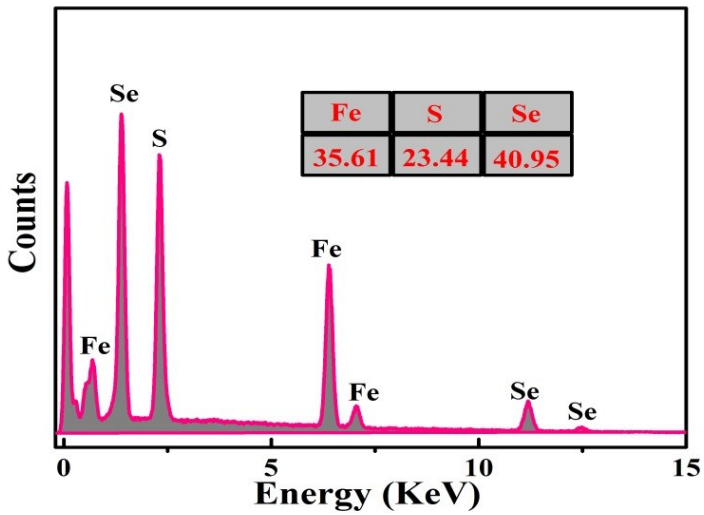

Fig. S1. EDS spectrum of FeS_2@$FeSe_2$ microspheres.

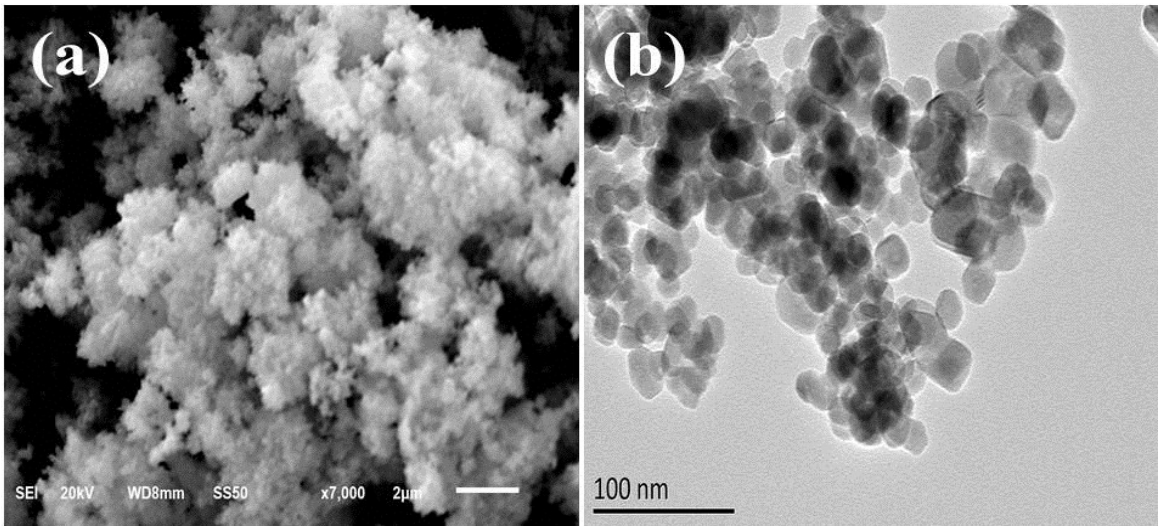

Fig. S2. SEM (a) and TEM (b) images of $FeSe_2$ nanoparticles, respectively.

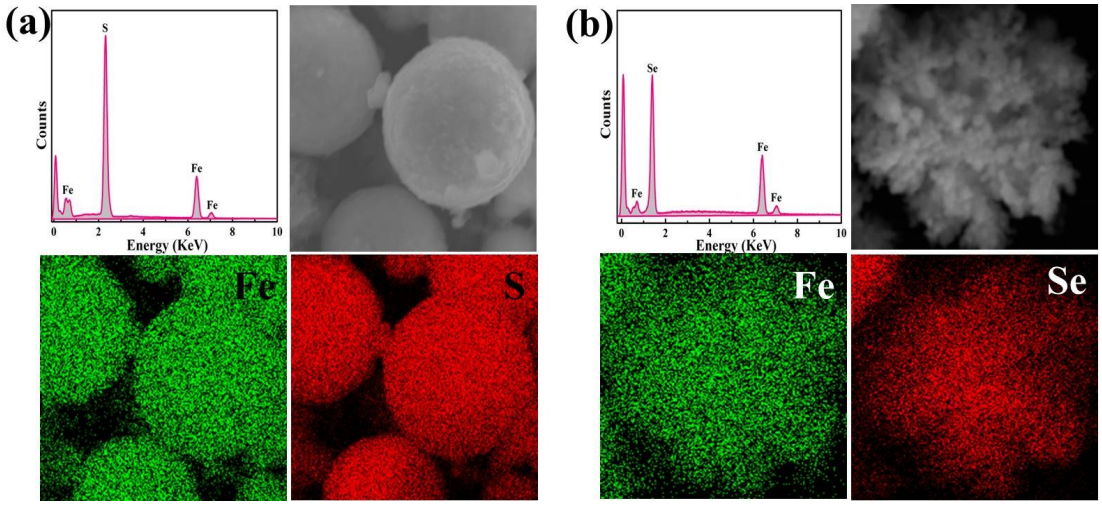

Fig. S3. (a, b) EDS spectra and elemental mapping of FeS_2 microspheres and $FeSe_2$ nanoparticles, respectively.

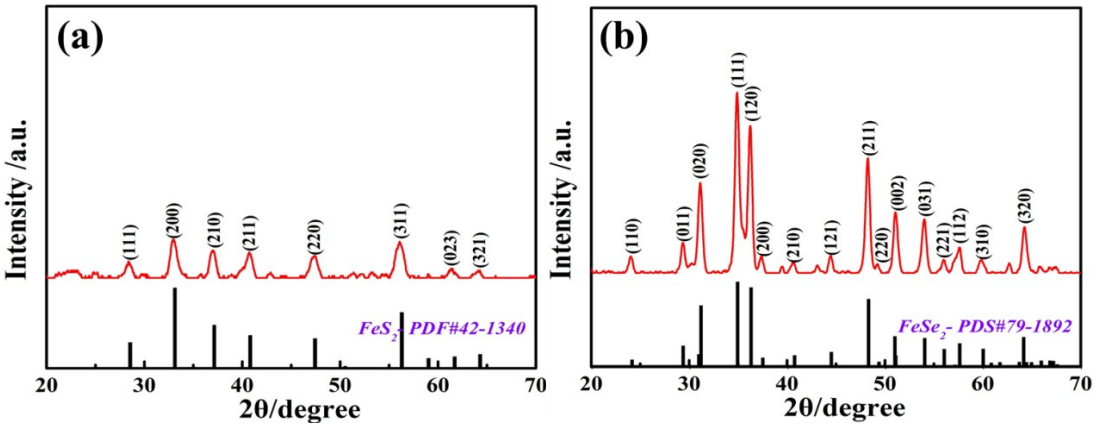

Fig. S4. (a, b) XRD pattern of FeS_2 microspheres and $FeSe_2$ nanoparticles, respectively.

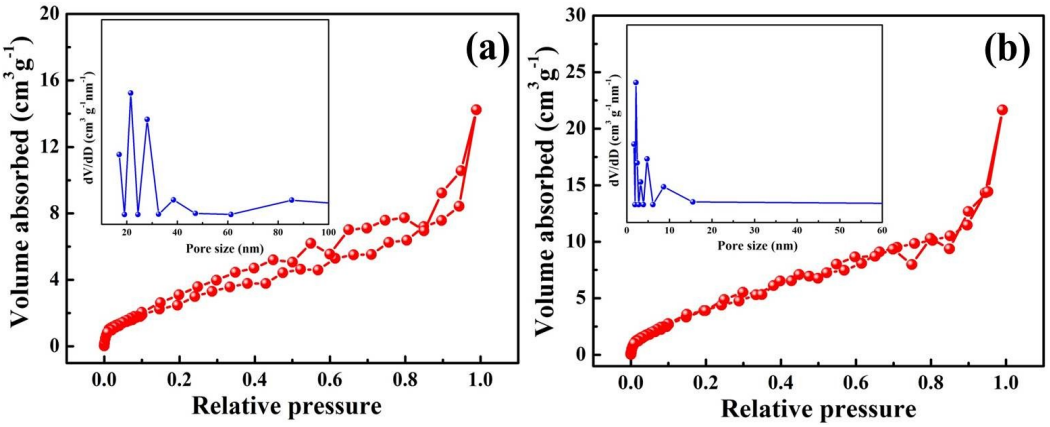

Fig. S5. (a, b) N_2 adsorption/desorption isotherms curves and BJH pore size distribution of FeS_2 microspheres and $FeSe_2$ nanoparticles, respectively.

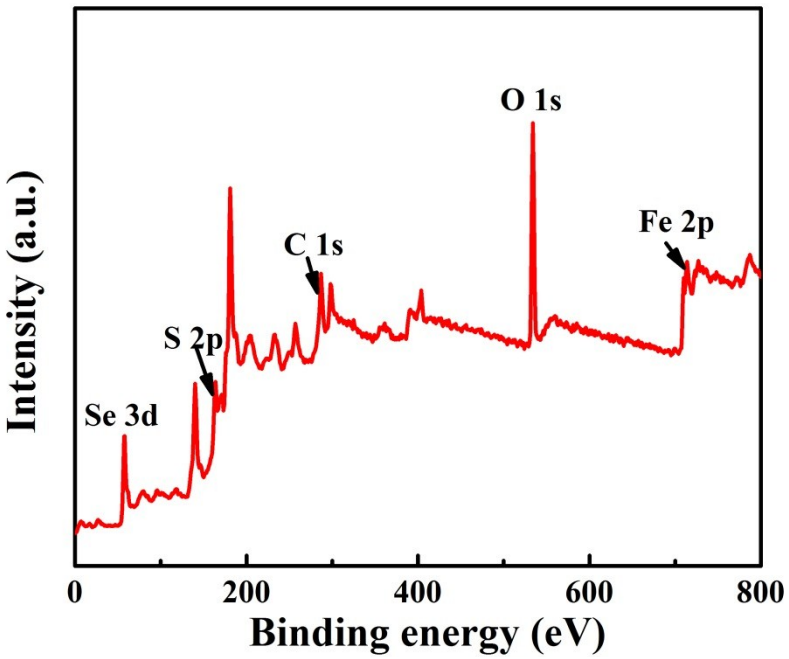

Fig. S6. XPS survey spectrum of FeS_2@$FeSe_2$ microspheres.

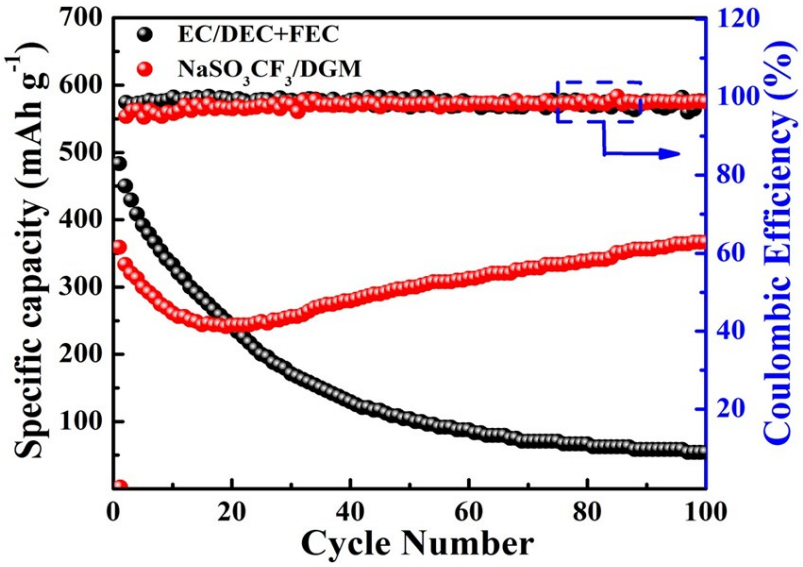

Fig. S7 The compassion of cycling performance for FeS_2@$FeSe_2$ electrode with ether- and carbonate-based electrolyte at a voltage windows of 0.5-2.9 V at 1 A g^{-1}.

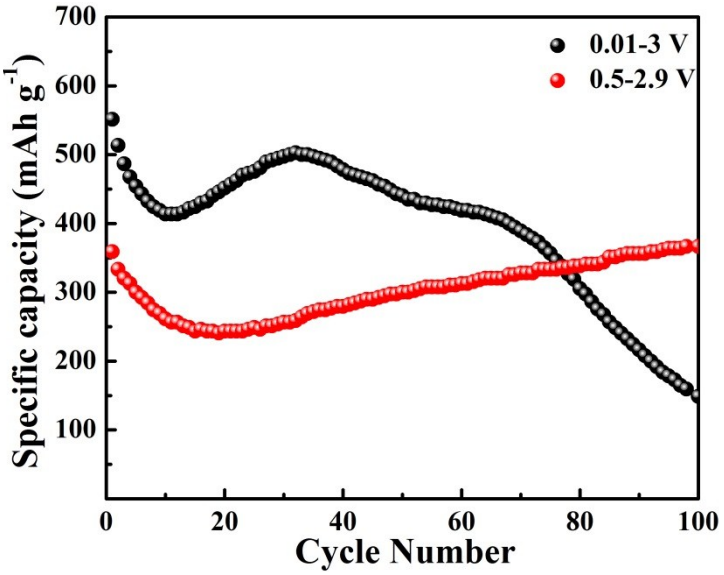

Fig. S8 The compassion of cycling performance for FeS_2@$FeSe_2$ electrode at a voltage windows of 0.5-2.9 V and 0.01-3 V at 1 A g^{-1}.

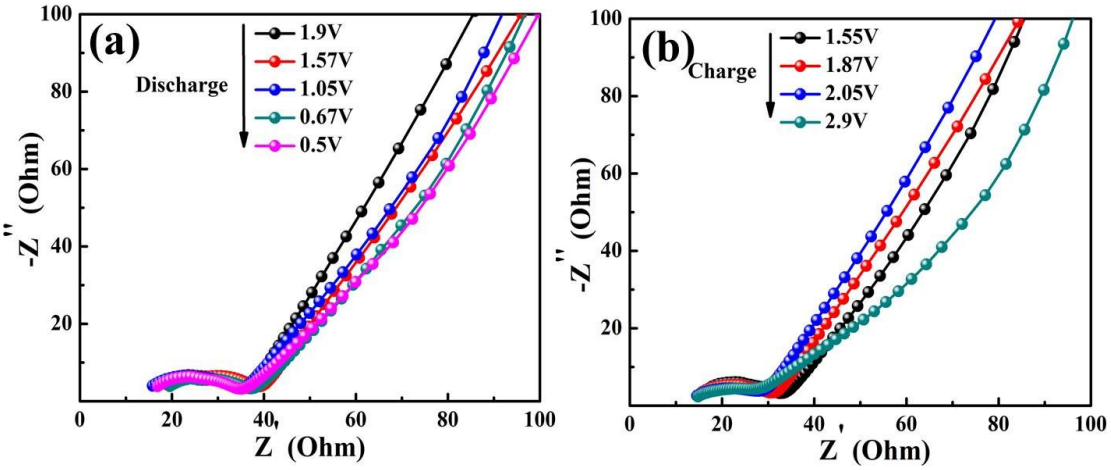

Fig. S9. (a, b) Nyquist plots of FeS_2@$FeSe_2$ electrode at different discharged and charged state with the frequency range from 100 kHz to 0.01 Hz, respectively.

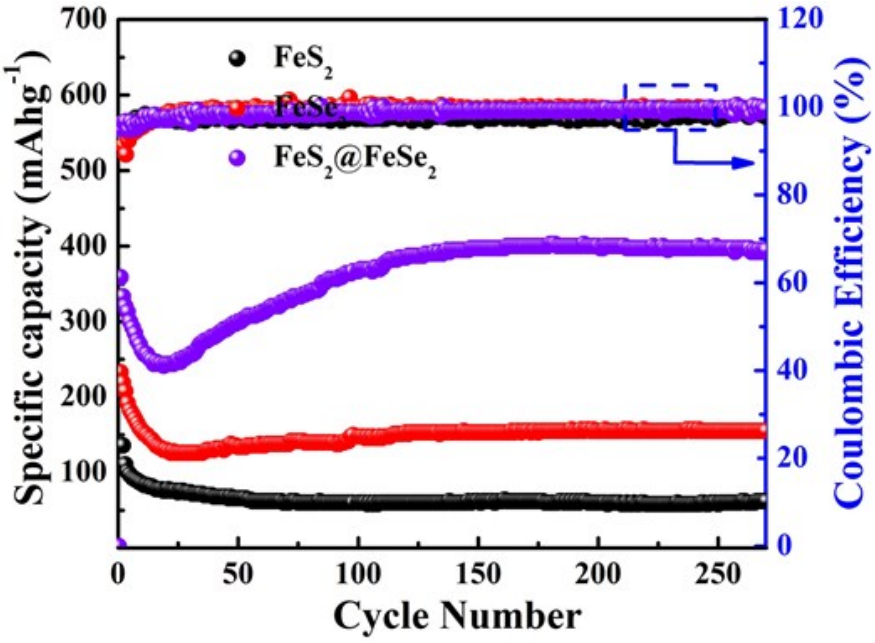

Fig. S10. The compassion of cycling performance for FeS_2@$FeSe_2$, FeS_2 and $FeSe_2$ electrode with potential range from 0.5 to 2.9 V at 1 A g^{-1}.

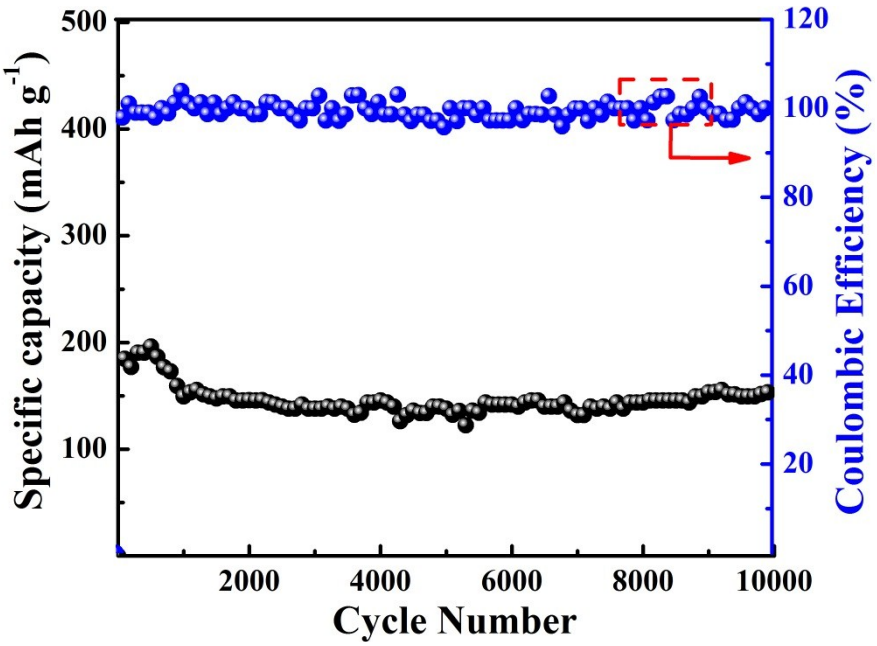

Fig.S11 Cycling stability test of the FeS_2@$FeSe_2$ electrode at 7 A g^{-1}.

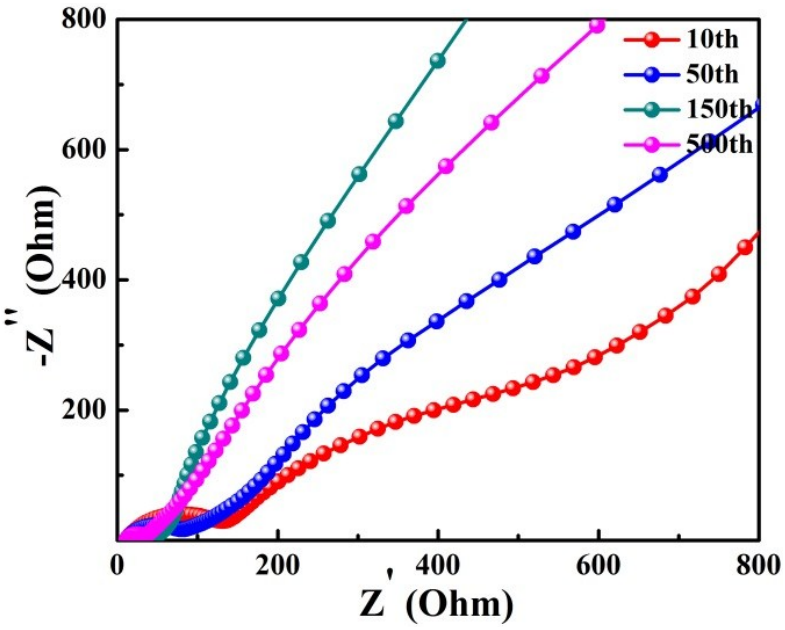

Fig. S12. Nyquist plots of FeS_2@$FeSe_2$ electrode after different cycles.

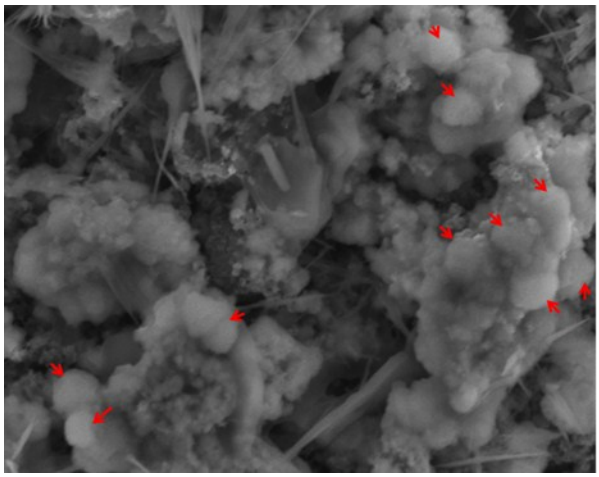

Fig. S13 The SEM image of FeS_2@$FeSe_2$ at 1 A g^{-1} after 200 cycles.

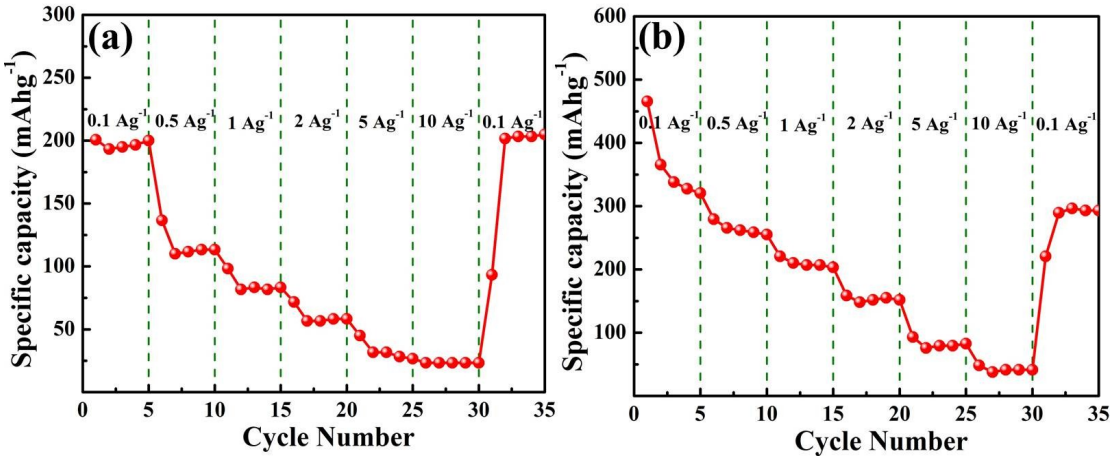

Fig. S14. (a, b) Rate capability measurement of plain FeS_2 and $FeSe_2$ electrode, respectively.

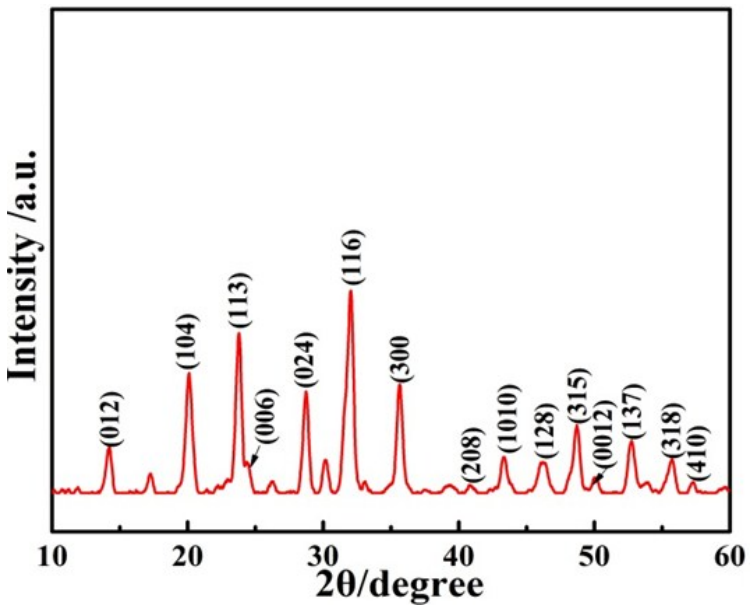

Fig. S15. XRD pattern of the $Na_3V_2(PO_4)_3$/C sample.

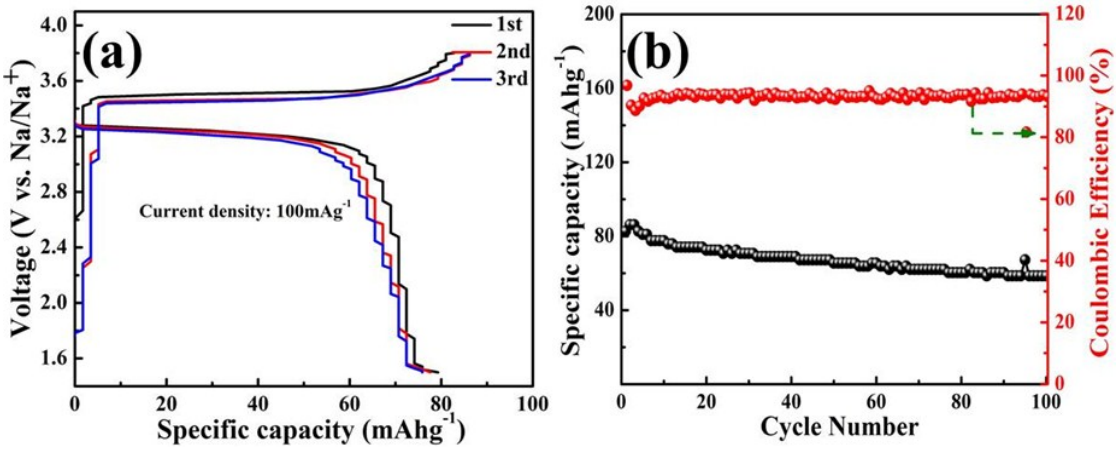

Fig. S16. Discharge-charge profiles of the $Na_3V_2(PO4)_3$/C electrode at first three cycles with a potentials windows of 1.5 ~ 3.8 V at 100 mA g^{-1}, (b) Cycling stability measurement of the $Na_3V_2(PO_4)_3$/C electrode at 100 mA g^{-1}.

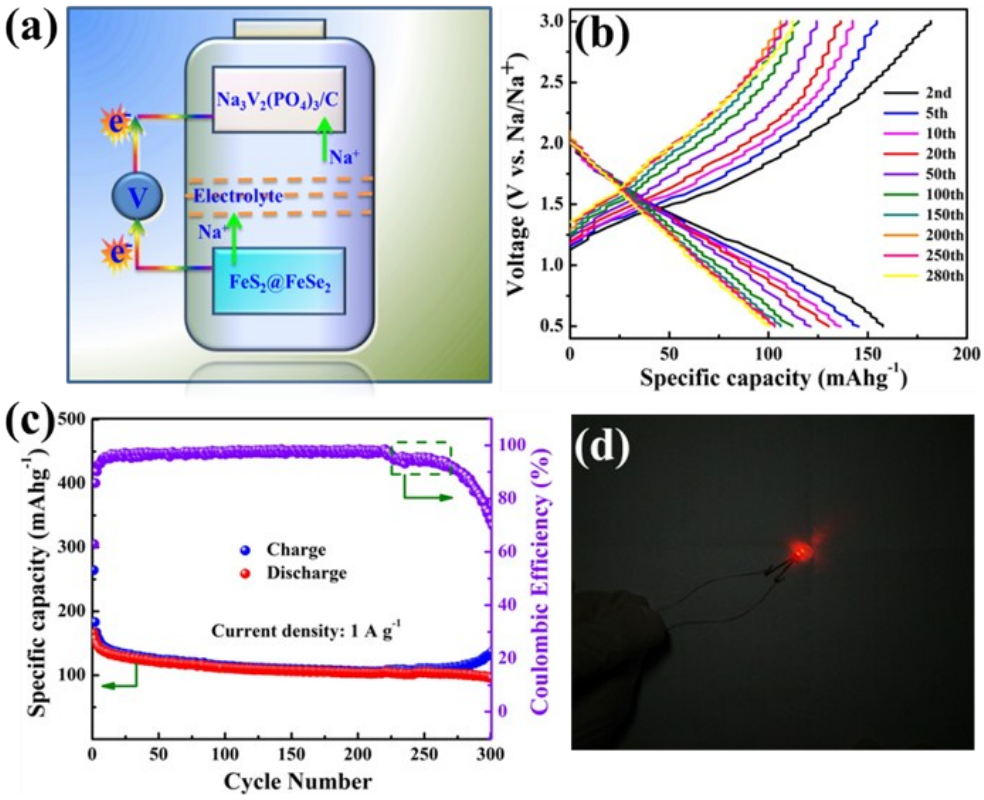

Fig. S17. $Na_3V_2(PO_4)_3/C$~ $FeS_2@FeSe_2$ full cell Configuration, (a) Schematic representation, (b) Discharge-charge profiles at different cycles, (c) Cycling performance at 1 A g^{-1}, (d) Optical image.

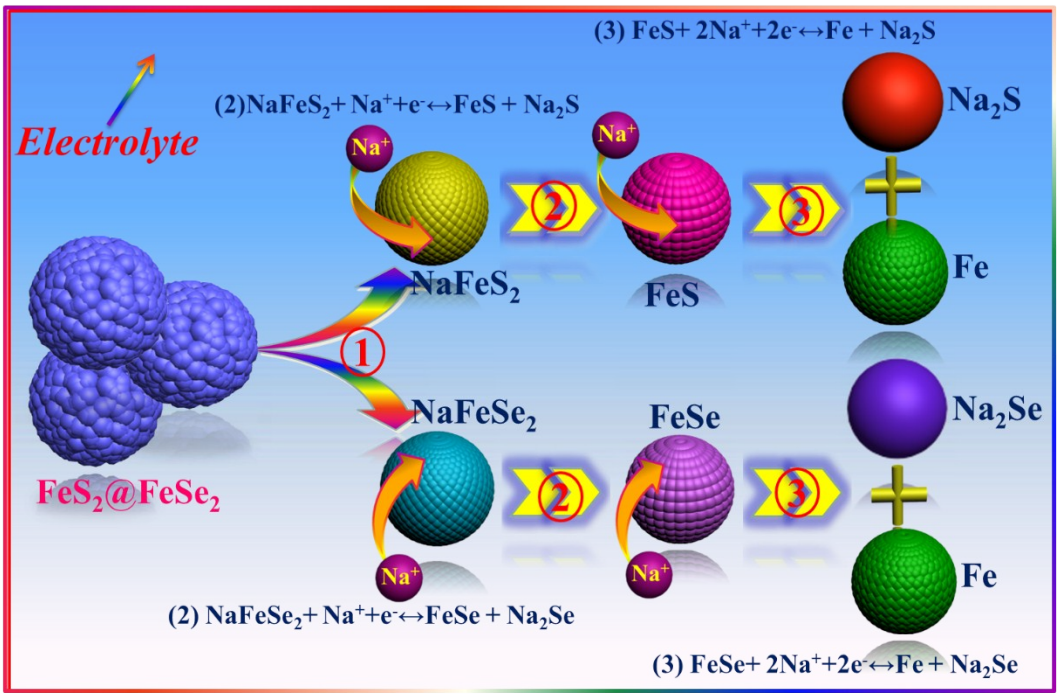

Scheme S1. Schematic illustration of reaction mechanism of FeS_2@$FeSe_2$ electrode during the sodiation and desodiation process.

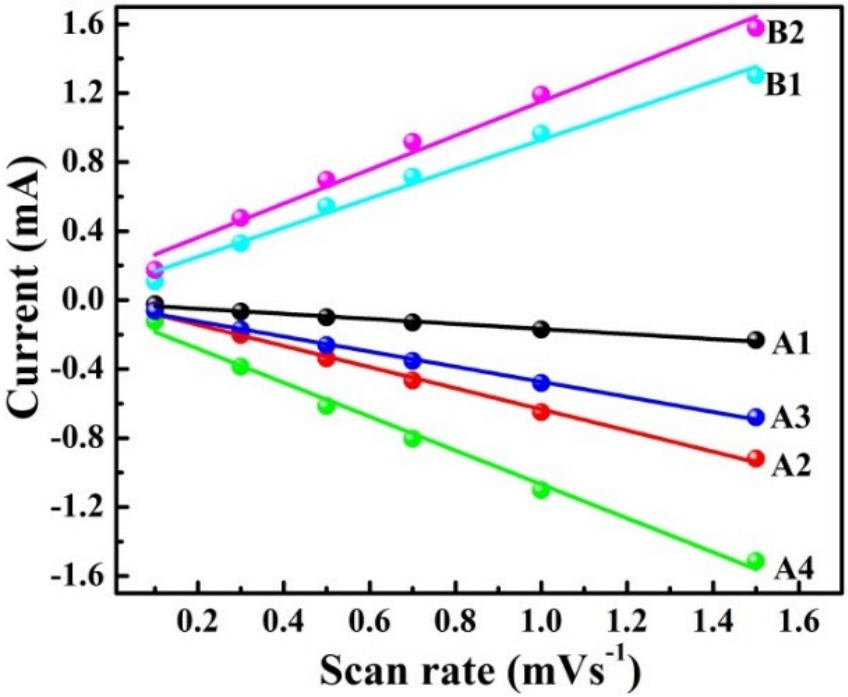

Fig. S18. Function relationship of current response (*i*) *vs.* scan rate (*v*).

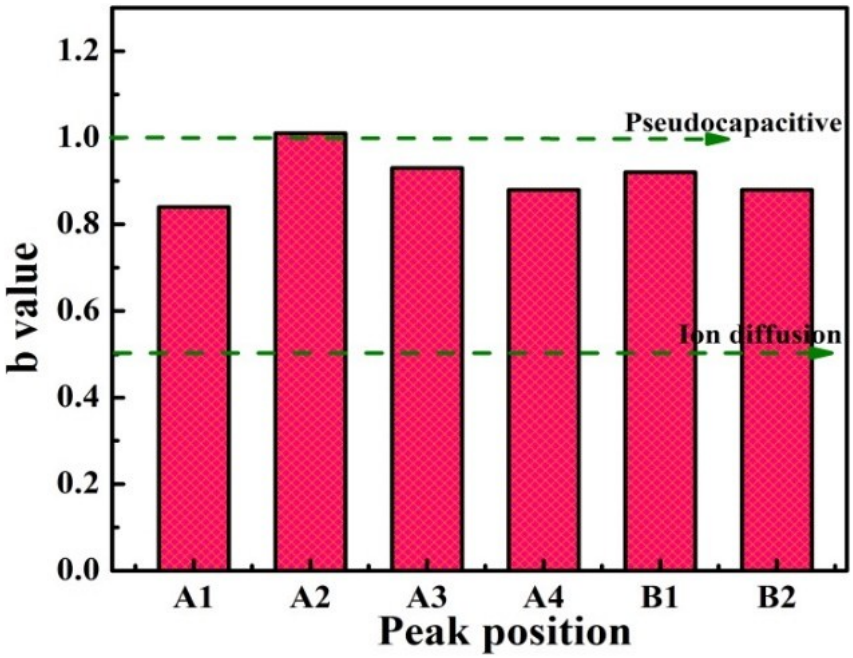

Fig. S19. Calculated b values at different peak position for FeS_2@$FeSe_2$ electrode.

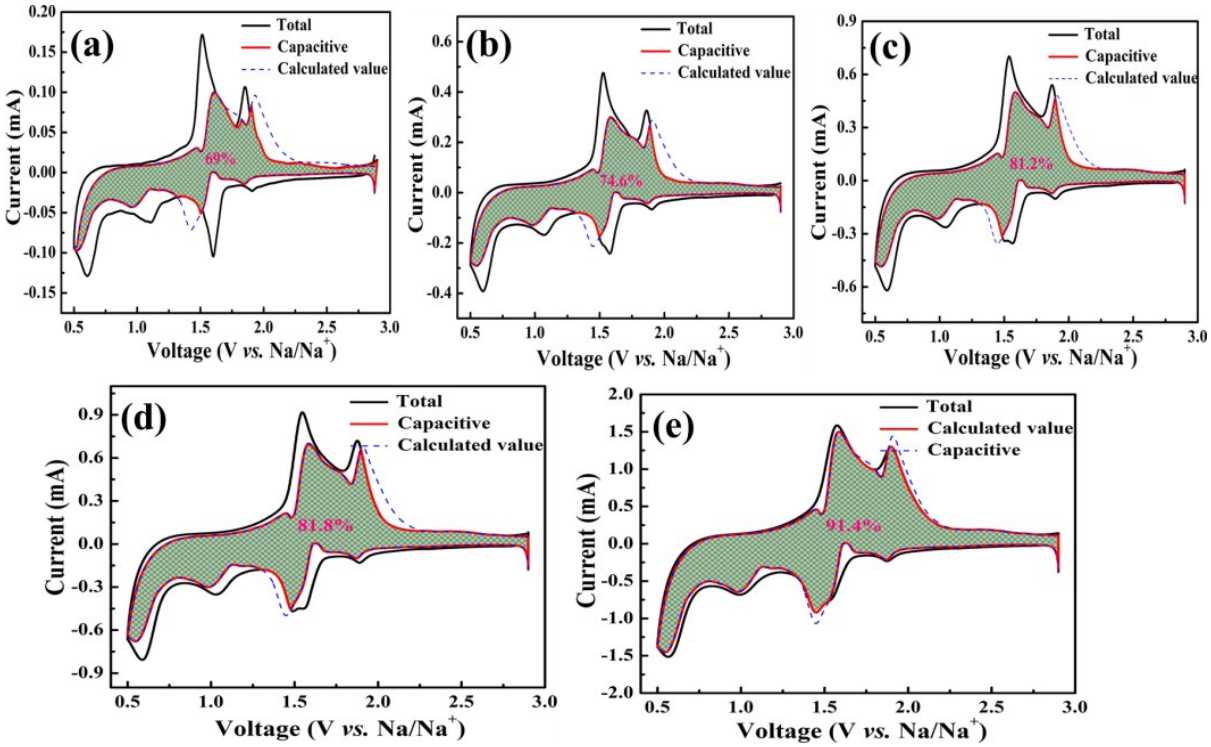

Fig. S20. Different CV curves of the FeS_2@$FeSe_2$ electrode with the pseudocapacitive contribution to the total current shown by the shaded part. (a) 0.1 mV s^{-1}, (b) 0.3 mV s^{-1}, (c) 0.5 mV s^{-1}, (d) 0.7 mV s^{-1}, (e) 1.5 mV s^{-1}.

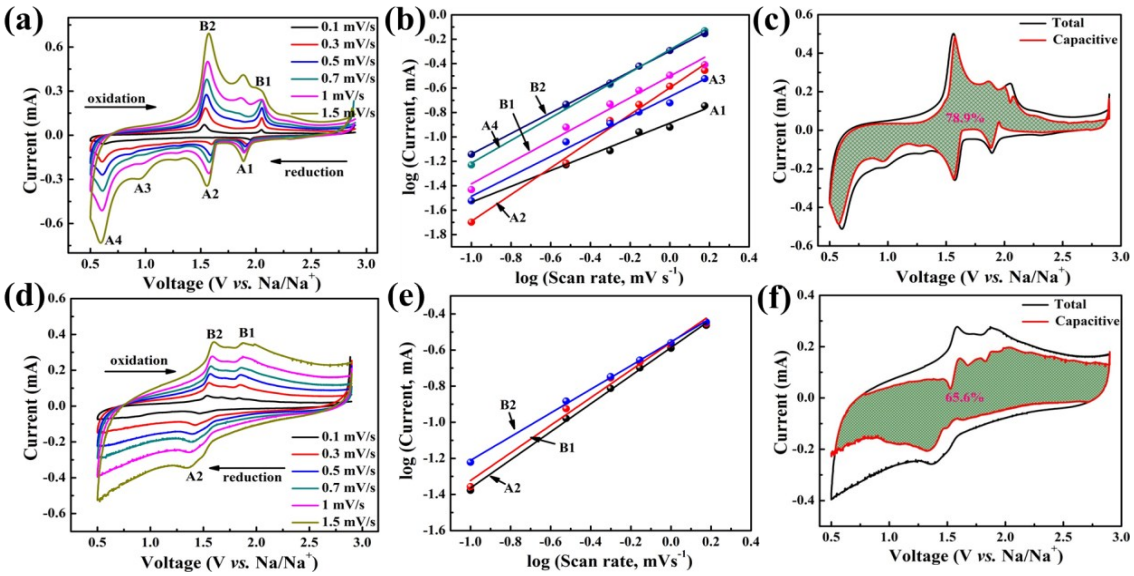

Fig. S21. CV curves of the electrode at different scan rates from 0.1 to 1.5 mV s^{-1}, (a) $FeSe_2$, (d) FeS_2 ; Log(i) *vs.* log(v) plots at each redox peak. (b) $FeSe_2$, (e) FeS_2; Different CV curves of the FeS_2@$FeSe_2$ electrode with the pseudocapacitive contribution to the total current shown by the shaded part at 1 mV s^{-1}, (c) $FeSe_2$, (f) FeS_2.

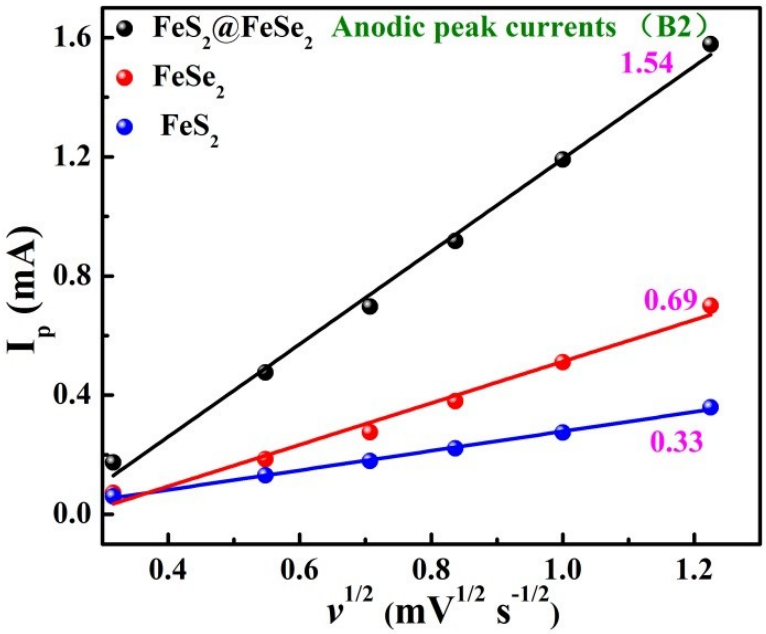

Fig. S22. Liner relationship between the peak current (I_p) and square root of the scan rate ($\upsilon^{1/2}$) of FeS_2@$FeSe_2$, FeS_2 and $FeSe_2$, respectively.

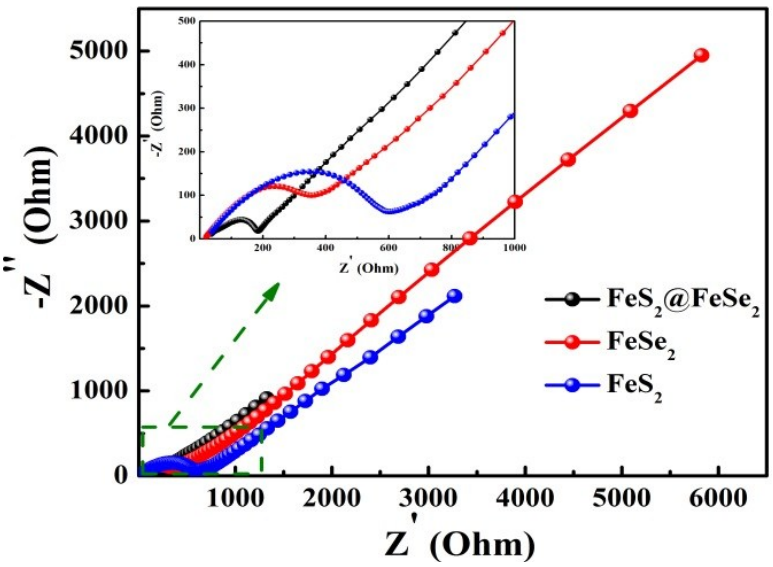

Fig. S23. Nyquist plots of FeS_2@$FeSe_2$, FeS_2 and $FeSe_2$.

Table S1. b-values at each redox peak of the $FeSe_2$ and FeS_2 samples

Samples	A1	A2	A3	A4	B1	B2
$FeSe_2$	0.62	1.07	0.85	0.94	0.87	0.84
FeS_2	N/A	0.78	N/A	N/A	0.77	0.66